IIETA International Information and Engineering Technology Association
Advancing the World of Information and Engineering

Journal of New Materials for Electrochemical Systems
Vol. 27, No. 3, September 2024, pp. 172-181
Journal homepage: http://iieta.org/journals/jnmes

Monitoring Atomic Layer Deposition by Potentiodynamic Electrochemical Impedance Spectroscopy of Multielement Adlayers

Hemlata Vikrant Ganvir[1], Sandeep Kumar[2], Rahul Kumar[3], Barun Haldar[4], Satishkumar Palanisamy[5]*, Ravi Verma[6], Dhananjay R Dolas[7], Vijayakumar Arun[8], Varsha D. Jadhav[9], Mayakannan Selvaraju[5]

1Department of Applied Physics, Yeshwantrao Chavan College of Engineering, Nagpur, India
2Division of Research and Development, Lovely Professional University, Phagwara, Punjab, India. 2University Centre for Research and Development, Chandigarh University, Mohali, Punjab, India
3Graphic Era (Deemed to be University), Clement Town Dehradun, Dehradun 248002,India
4Assistant Professor, Mechanical and Industrial Engineering Department, College of Engineering, Imam Mohammad Ibn Saud Islamic University (IMSIU), Riyadh-11432, Kingdom of Saudi Arabia
5*Department of Mechanical Engineering, Rathinam Technical Campus, Coimbatore, Tamil Nadu, India
6Assistant Professor, School of Computing Science and Engineering, VIT Bhopal University, Kothrikalan, Sehore, Madhya Pradesh, India
7Mechanical Engineering, Jawaharlal Nehru Engineering College, MGM University, Aurangabad, Maharashtra, India
8Department of Electrical and Electronics Engineering, Mohan Babu University, Tirupati, India
9Department of Artificial Intelligence and Data Science, Vishwakarma Institute of Technology, Pune, Maharashtra, India.

Corresponding Author Email: sp.sathishkumar10@gmail.com

https://doi.org/10.14447/jnmes.v27i3.a02

Received: 30/01/2024
Accepted: 10/08/2024

Keywords:
Underpotential deposition, Layer-by-layer deposition, PDEIS, Metal-chalcogen multilayer, equivalent electric circuits (EEC)

ABSTRACT

Atomic multilayer assembly monitoring is now possible using a method that has been extended from multiparametric characterization of changeable electroactive interfaces using potentiodynamic electrochemical impedance spectroscopy (PDEIS). The multilayers were created by depositing adlayers of Sb, Se, and Sn on Ag in a sequential fashion, and by depositing an adlayer of Zinc on an antimony underlayer that was supported by Silver. The multilayers were characterized using the potentiodynamic mode, which utilizes the relationship between AC circuit characteristics and electrode potential. The dependences show changes in the double electric layer at the interface, and in diffusion and charge transfer. While Ag/Sbad/Sead/Agad and Ag/Sead/Agad exhibit considerable similarity in the Faradaic part of the ac response, the dependencies of the distinctive variables of the Ag/Sbad/Sead/Snad (Ag/Sbad/Sead/Snad) composite threelayer differ significantly from those of the Ag/Sbad/Snad and Ag/Sead/Snad bilayers, respectively. The adlayer oxidation potential shifts dramatically when tin is deposited on a bi-chalcogen Ag/Sbad/Sead underlayer, proving that the upd of Sn, Ag, and Zn on chalcogen adlayers is irreversible. Silver can partially dissolve in the Ag adlayer oxidation potential when it penetrates the Ag/Sbad/Sead bilayer, unlike the Sn adlayer that forms on top of the Antimony-selenium bilayer and dissolves completely in the anodic scan within the stability scope of the chalcogen composite underlayer. Electrochemical nanotechnologies can utilize PDEIS for monitoring layer-by-layer deposition by leveraging the self-descriptive nature of potential dependences of circuit variables..

1. INTRODUCTION

Underpotential deposition is the surface-limited electrochemical deposition that can create atomic adlayers when the electrode potential is higher than the potential for bulk phase formation. These adlayers have potential uses in semiconductor heterostructure preparation, electrochemical atomic layer epitaxy, and nano colloids [1], [2], [3]. Using underpotential deposition, substrates with a wide range of geometries can have atomic layers deposited upon them. The technological potential of upd is limited, however, monitoring techniques that are practically possible for atomic layers only accessible in smooth surfaces.

In simple systems, monitoring upd by direct current is self-explanatory. Cathodic and anodic scans exhibit ideal current peaks in classical instances of upd [4], [5]. It becomes more difficult to monitor under prospective deposition when metal ions are decreased on a pre-deposited atomic layer of alternative component. An example of this is the fact that a silver electrode coated with an antimony atomic adlayer (Sb_{ad}) will not exhibit an upd peak for silver, whereas a silver electrode coated with bare silver will display flawless current peaks [6]. Despite this, surface limited mode Ag_{ad} deposition is still possible, and the creation of the $Ag/Sb_{ad}/Ag_{ad}$ bilayer may be confirmed by visible peaks corresponding to the consecutive anodic oxidation of the Ag_{ad} and Sb_{ad} adlayers.

Materials with atomic layers or several layers can be electroactive. To fully understand the dynamics of upd, it is necessary to monitor more than one dependent variable due to the fact that atomic layer deposition drastically alters the electrochemical interface's chemical and electric condition. Because the electrochemical interface's chemical composition influences the double layer's capacity during atomic layer deposition, the charging current is potential-dependent. However, this is frequently underestimated in up-to-date investigations that only use cyclic voltammetry (CV) to monitor a single dependent variable. Potentiodynamic electrochemical impedance spectroscopy (PDEIS) analysis of several upd techniques has revealed that upd frequently results in highly noticeable variations in double layer capacitance (Cdl)[7], [8], [9]. The total current measured by CV might be affected by other processes, such as the co-adsorption of anions and the bonding between different adlayers components. As a result, electrochemical atomic layer deposition potentiodynamic monitoring requires a multiparametric strategy.

Although cyclic voltammetry's potentiodynamic mode is well-suited to upd, classical CV, which only monitors a single dependent variable, frequently can't tell the difference between multiple concurrent processes. Because the ac response is two-dimensional and real and imaginary impedance depend on different frequencies, multifrequency ac probing is perfect for characterizing many processes on the same interface at the same time [10]. In quasi-linear potential scans, PDEIS obtains the potential-dependent impedance spectra, and this method proved to be self-descriptive when characterizing different atomic layers in underpotential deposition[11], [12]. Analysis of potentiodynamic electrochemical impedance spectroscopy spectra in terms of equal electric circuits typically yields multiple potential functions describing differences of the double layer, diffusion of electroactive particles, interfacial charge transfer and co-adsorption of anions, capacitor of adsorption.

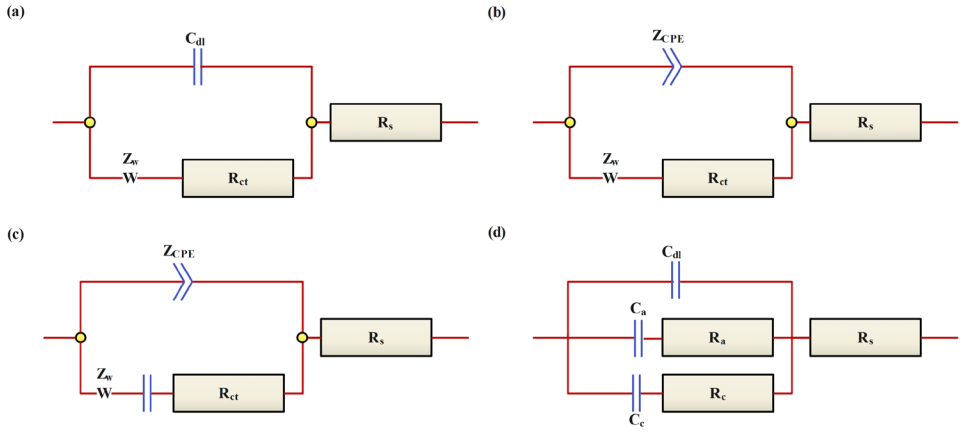

Figure 1. EEC for various PDEIS scenarios

Fig. 1 displays the circuit of electrochemical systems with equivalent underpotential deposition. The physical significance of the components of these circuits is highly apparent. A series of obstacles in most cases, solution resistance is the root cause of R_s. Although this component is not directly related to the interface, it must be considered in order for other components of the EEC to be calculated. As a result of upd's impact on the interface status, double layer capacitance (C_{dl}) is among the most sensitive upd indicators.

The phase shift in the ac response is typically more accurately recorded in PDEIS than the ac amplitude, and C_{dl} is typically the main contributor to this shift. When dealing with nonstationary interfaces, the double layer typically exhibits slightly different behavior than an ideal capacitor. In this case, the phase shift may be slightly lesser than 90˚, but its contribution remains frequency independent across multiple orders of magnitude. This type of EEC element is known as a constant phase element and the subsequent equation defines its impedance, Z_{CPE}[13], [14]:

$$Z_{\mathrm{CPE}} = Q_{\mathrm{dl}}^{-1}(j\omega)^{-n} \qquad (1)$$

The physical meaning of Q_{dl} is determined by the exponent n, where ω represents the circular frequency and j is the imaginary unit. As the quantity Q_{dl} approaches 1, it transforms into capacitance and can be seen as pseudo-capacitance. The $C_{dl}(E)$ shows the state of the double layer, the relationship between Q_{dl} and the electrode potential can be utilized as an sign of the same when n approaches one [15].

The reversibility of the upd is the primary determinant of the possible combinations of EEC elements that characterize the Faradaic half of the ac response, which is the portion of the equal circuit that is in parallel with C_{dl} or Q_{dl}. The corresponding circuit's capacitance-like effect on the producing ac current is analogous to the oscillations' effect. During reversible underpotential deposition, the fluctuation of the potential results in the adatom reporting on the electrode surface oscillating. Due to its roots in kinetics, the resultant adsorption capacitance C_{ads} is a useful metric for characterizing upds; for instance, the EEC with Cads illustrated in Fig. 1c was employed to describe the phase transition in Sn underpotential deposition on Au [16]. The adsorption of cations and anions, which are mutually correlated and can be observed in a single potential scan. For example, when Ag and Bi are adsorbed on Au in sulphuric and perchloric acids, two adsorption capacitances are produced in parallel [17], [18].

This research focus on irreversible upd, which does not have a capacitor in the equal circuit's Faradaic branch. Irreversible upd's equivalent electric circuits resembles a standard Randles

circuit (Fig. 1a), however, CPE is often used to depict the double layer (Fig. 1b) [19], [20]. The following relationship between Z_W and circular frequency is given by the semi-infinite diffusion model, which typically agrees with the following values for R_{ct} and Z_W, the impedance of diffusion:

$$Z_{\mathrm{W}} = \frac{A_{\mathrm{W}}}{(j\omega)^{0.5}} \quad (2)$$

Here, A_w is the Warburg coefficient, and this is helpful for following the Faradaic ac response that is governed by diffusion.

The simple structure of the interfacial layer enables the thorough analysis of the AC response of underpotential deposition in Potentiodynamic electrochemical impedance spectroscopy. Despite certain changes to the double layer caused by upd, the additivity of the double layer charging and the Faradaic current remains mostly unaffected, and the Warburg element well describes diffusion. There is an expected and easily interpretable variance in the equivalent circuits across the various upd systems [21], [22]. Hence, PDEIS in conjunction with equivalent electric circuits analysis showed potential as a method for independently tracking the double layer, diffusion, charge transfer and adsorption processes all at once. Furthermore, it is worth noting that the potentiostat, which is often utilized for regulating electrochemical deposition, is also employed to acquire PDEIS spectra. Experimental procedures in PDEIS and cyclic voltammetry are quite similar to those in potentiodynamic impedance spectroscopy, which involves superimposing a quasi-linear potential scan on top of a tiny ac perturbation (often ranging from 5 to 10 mV).

This research builds on earlier work in multiparametric characterization of various atomic layer depositions and applies the same methodology to layer-by-layer gathering and characterization of atomic layers consisting of 2 or 3 components. Here, we employ a building block of $Ag/Sb_{ad}/Se_{ad}$ consisting of the two chalcogen adlayers, as opposed to the bimetallic $Ag/Sb_{ad}/Ag_{ad}$ /Sn_{ad} three-layer that was previously reported [23]. The Sn and Ag upd utilized this block as its underlayer. Diverse chalcogen-chalcogen and chalcogen-metal effects have been seen in the Faradaic and double layer responses of the ac response when these parts are studied independently. Assembling many layers seems to give PDEIS and self-descriptive multidimensional picture of the electrochemical contact response.

2. EXPERIMENTAL METHODOLOGY

The electrodes used in each experiment, which were made of polycrystalline silver wire were flame annealed and then cooled in air. Before the adlayer deposition, the electrodes were cycled in 0.1M HClO4 to ensure a consistent surface state, ranging from -400 to 900mV. The following solutions were used to develop the multilayers: 1mM SbO_2 +0.1M $HClO_4$ (Sb underpotential deposition), 1mM selenium oxide +0.1M perchloric acid (Se underpotential deposition), 1mM tin (II) perchlorate +0.1M perchloric acid (Sn underpotential deposition), and 10mM $Ag(ClO_4)_2$ +0.1M perchloric acid (Ag underpotential deposition).

The layers were then deposited on a $0.024cm^2$ Au electrode in a sequential fashion. Two layers of Sb_{ad}, made of 2mM SbO_2 +0.1M HCl +0.1M KCl, and two layers of Zn_{ad}, made of 3mM $ZnCl_2$ +0.1M HCl +0.1M KCl were successively positioned on a $0.02cm^2$ Au electrode to form an $Ag/Sb_{ad}/Zn_{ad}$ bilayer. The surface area of the Au electrode was measured using oxygen electrochemical adsorption, following the method [24].

The employed electrode was washed with the appropriate blank solution after each deposition stage and then immersed in the subsequent working solution. Using the same methods, previous research [25], [26] discovered that the atomic layers of Sb and Se remained undamaged.

No air was introduced into the working solutions by means of nitrogen. A three-electrode electrochemical cell was utilized to isolate reference electrode from the working solution. The Sb_{ad}/Se_{ad} bilayer was created on Ag by depositing selenium on an antimony atomic underlayer using surface restricted deposition at 240 mV. We found that the deposition ranged from 150 mV to 250 mV under potentiostatic control, which falls within the restrictions on bulk selenium deposition on bare Au [27]. This suggests that the deposition was surface limited. The electrode covered with Sb_{ad} didn't show the Se underpotential deposition peak or the peak of restricted bulk selenium deposition in CV, unlike the bare Ag electrode; however, bulk selenium deposition did occur below 150mV. With an electrode holding period of up to 1 minute in the potential scope of 150mV to 250 mV, the anodic peak of Se_{ad} steadily grew due to the sluggish kinetics of selenium deposition on Ag/Sbad. To get the sustained amount of Se_{ad}, we utilized a 2-minute deposition at 240 mV. Through CV testing, we were able to confirm that the Se_{ad} deposition on Sb_{ad} was thorough and that no bulk Se phase was present.

By analyzing 19 wavelets in real-time at every 3mV step of a staircase potential ramp, Potentiodynamic electrochemical impedance spectroscopy spectra obtained from frequency scope of 20 Hz to 900Hz. A built-in spectrum analyzer of the potentio-dynamic electrochemical impedance spectroscopy spectrometer was used to do the spectrum analysis[28], [29]. This analyzer provided a best-fit equivalent electric circuits and displayed its variables as functions of the potential. The equal circuit displayed in Figure 1b fitted all the spectra and allowed for the separate examination of the double layer (Q_{dl}), diffusion (Aw),and interfacial charge transfer (R_{ct}), a potential-dependent variable of the Warburg impedance ZW, because the upd processes are irreversible. The PDEIS experiment and fitting process are described in more depth [30].

3. ANALYSIS OF PDEIS SPECTRA AND INITIAL ASSESSMENT

The potentiodynamic electrochemical impedance spectroscopy spectra of Sn and Ag upd on the $Ag/Sb_{ad}/Se_{ad}$ composite underlayer, and the potentiodynamic electrochemical impedance spectroscopy spectra of Zn upd on Sb_{ad}, are displayed in Fig. 2a-c. Hundreds of common impedance spectra compose two surfaces that make up each PDEIS spectrum. Figure 2d displays four instances of the second type in Nyquist coordinates. The PDEIS spectrum is color-coded, with red lines representing cathodic processes and

blue lines representing anodic processes. The colored lines connect areas of same frequency in Nyquist plots associated with similar scan direction.

From Fig. 2, it is evident that there is a distinct contrast in the spectra between the cathodic and anodic scans. The cathodic and anodic portions of Potentiodynamic electrochemical impedance spectroscopy spectra demonstrate distinct interface states at various atomic layer deposition and oxidation stages, much like the cathodic and anodic branches in CV. The potentiodynamic mode is essential for voltametric examination of underpotential deposition due to the absence of a peak in the stationary voltammogram. Similarly, when testing the potentiodynamic frequency response, the Potentiodynamic electrochemical impedance spectroscopy spectrum, rather than being seen as a collection of distorted stationary impedance spectra, that can interpret as multidimensional property of unfixed state along the process trajectory of atomic layer formation and destruction. In a similar vein, the spectra-derived parameters that will be detailed later on in this article define the ac response components associated with a particular interfacial item at various stages of the process. Charge transfer (resistance Rct), diffusion of electroactive particles, and the double layer denoted in the equivalent electric circuits by impedances ZW and ZCPE can all be characterized by examining the spectra displayed in Figure 2, which are part of the best-fit EEC displayed in Figure 1b. Dependences on the potential of the Warburg coefficient Aw and parameter Qdl of the constant phase element have been used to describe the change of the two later components. The other ZCPE parameter, the exponent n, was in the scope of 0.9 - 1, positioning the constant phase component physically near a capacitor. For values of n that are sub-1.0 We refer to the parameter Qdl as pseudo-capacitance since the phase shift is slightly smaller. Note that there is an additional physical quantity known as pseudo-capacitance-adsorption capacitance. It is derived from chemicals however, when considering the AC response, it is actually a true capacitance (it produces a 90◦ phase shift). While Qdl is genuinely capacitive (it comes from the double layer capacitor), it is also pseudo-capacitor because it describes the equivalent electric circuits component with phase shift that is slightly less than accurate capacitance. The interface nonstationary likely explains why n is not precisely equal to 1.0 in the majority of updated processes; this causes the double layer to operate slightly differently from an ideal capacitance. In contrast to stationary impedance spectroscopy, PDEIS determines the EEC by analyzing frequency responses across a more limited frequency range. Therefore, Potentiodynamic electrochemical impedance spectroscopy does not confirm whether an element is present or not, thus it is theoretically conceivable to "overlook" an element that is only present in the response at very low or high frequencies. By varying their inherent variables in the potential scan, the various interfacial objects (such as charge transfer and double layer) can be identified and their contributions to the acquired multifrequency ac response can be broken down using PDEIS's circuit analysis. Instead of checking if the EEC would stay the same across all frequencies, PDEIS uses a complicated nonlinear regression method to accurately analyze the spectrum that is actually usable [31]. PDEIS comprehensively evaluates every aspect of the response. By analyzing hundreds of two-dimensional impedance spectra in single spectrum process, it is possible to obtain a more detailed understanding of the response. A more precise assessment of comparable circuit validity than would be possible with a single, perfectly recorded spectrum is made possible by this comprehensive study. Unlike a single 2D spectrum analysis, PDEIS's robust circuit analysis is the result of equivalent electric circuits testing at several group of circuit variables in potential scan.

Spectra displayed in Figure 2a-c show the combined effects of solution resistance, the three interfacial objects, and the real and imaginary impedance values. Images of the PDEIS spectra can be used to conduct a preliminary investigation of the interface difference in underpotential deposition, even though the impedance origin is complex. In a specific range of potentials, all three systems exhibit a significant drop in magnitude of imaginary impedanceZ'' in cathodic scan, but in the reverse scan, it increases at more positive potentials. Since the double layer capacitance is a major factor in irreversible upd and is substantially larger for metallic electrodes compared to chalcogen electrodes, this is partially explained by the fact that this phenomenon is highly transparent.

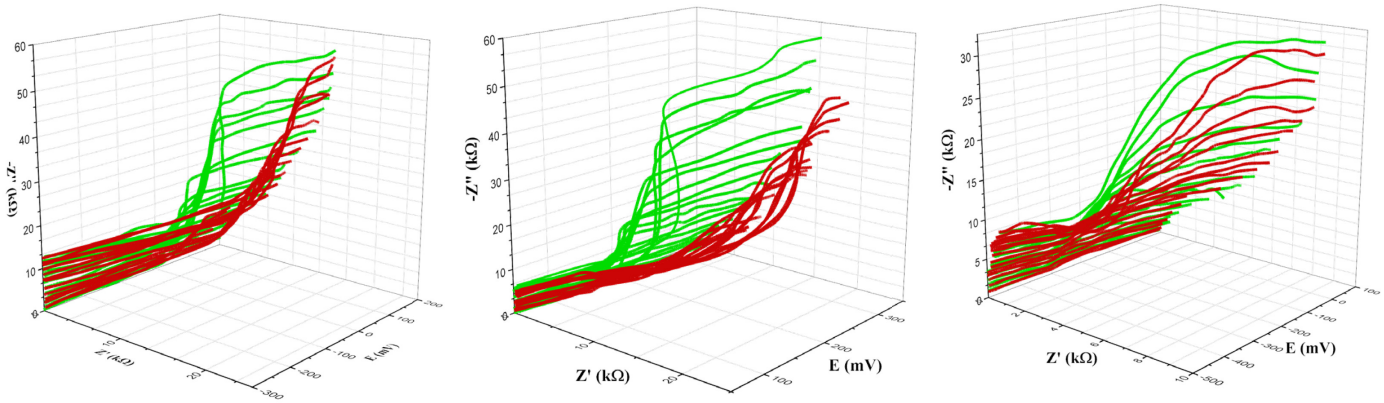

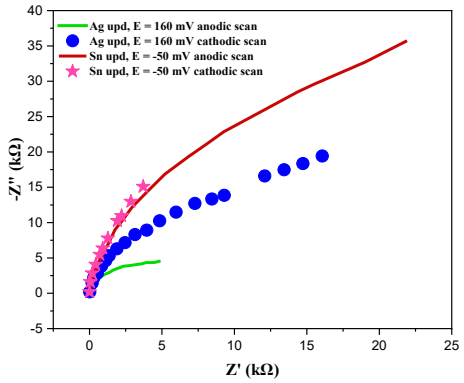

Figure 2. PDEIS spectra for Sn, Ag, and Zn on multilayer with constant potential segments.

It follows that an electrode surface terminated with a metal adlayer will have a larger imaginary impedance and a smaller capacitance than an Au crystal structure ended at the surface with Sb_{ad}/Se_{ad}. The spectrum picture confirms this prediction and reveals sharp Z-shifts at adlayer deposition and oxidation potentials. Next, we'll show quantitative data that back up the inference from the spectra and show how each of the three main factors affecting the multilayer assembly's variable interface ac response behaves individually.

The potentiodynamic voltammograms displayed in Figure 3 illustrate the various stages of the 3-component multilayer assembly on Silver, which consists of Ag, Sbad, Sead, and Snad. The voltammograms displayed cathodic peaks at around 340 mV due to the underpotential deposition of antimony and selenium. The oxidation potentials of Ag/Sbad and Ag/Sead are different by 200mV. For Sead, the anodic charges were 235Ccm−2, while for Sbad they were 285C cm−2. Typical for Sb adlayers generated in the potential range of their major underpotential deposition peak is a charge of 285C cm-2. Although a potential near to Sb bulk deposition could have allowed for more Sb to be put in a surface limited mode, we were able to avoid bulk deposition by restricting the deposition potential by 130 mV. Electromagnetic spectrum of Ag/Sbad/Sead collected by Sead deposition at 250 m. During the Sbad and Sead oxidation processes, V showed two anodic peaks; the antimony peak moved to higher positive electrode potentials, while the Sn peak moved marginally to further negative potentials when tested in contradiction of separate adlayers. The 505 cm−2 was anodic charge for Ag/Sbad/Sead. We found that varying scan rates resulted in the additive charge when Sbad and Sead deposition on Au was performed layer-by-layer. Composite Se-Sb adlayers, developed from perchloric acid solutions containing equal parts SbO2 and SeO2, showed significantly lesser anodic charges. Voltammetric data is not well suited for atomic multilayer characterization because the charges derived from it are sensitive to scan rates and solution composition. Although bi-chalcogen structure was placed layer-by-layer, infact that selenium and antimony charges are additive implies that there was no replacement interaction with antimony adlayer during selenium deposition.

Conducting selenium deposition at various potentials and then recording anodic stripping voltammogram allowed us to determine if bulk selenium deposition could impact the creation of the Ag/Sbad/Sead structure. The anodic voltammogram changed from 250 to 130mV as a result of the selenium deposition potential shift, as seen in curves 3,4 of Fig. 3a. A new anodic peak at about 630 mV shows that the bilayer now has a 3D selenium phase, and the anodic peak of Sbad moves to even additional positive potentials, clearly because the Se overlayer protects the antimony. To prepare the Ag/Sbad/Sead bi-chalcogen structure, the anodic peak of the Antimony adlayer must be high enough, but it can also change as selenium is deposited. Despite this, the anodic peak can still differentiate bulk selenium from Sbad.

Figure 3b shows that the underpotential deposition of Sn on Ag/Sbad/Sead is highly irreversible. In contrast to the Snad anodic oxidation on Ag/Sbad described by author [32], the composite bilayer's anodic oxidation (curve 4 in Figure 3b) moves to a greater positive potential. As shown in curve 5 of Figure 3b, anodic stripping exhibits three consecutive peaks that are ascribed to the oxidation of tin, antimony, and selenium. The anodic charge of Ag/Sbad/Sead bilayer was unaffected by stripping and cyclic deposition of the Tin adlayer, however the solution-based tin ions influence the potentials of selenium and antimony adlayer oxidation.

Determinations of equivalent electric circuits parameters (Fig. 4) derived from comparable PDEIS spectra provide a more in-depth look at the interface difference in Sn underpotential deposition and stripping on the bi-chalcogen underlayer. In Figure 4a, we can see the modification of the double-layer pseudo-capacitance Qdl during the hypothetical cycles of tin monolayer deposition and stripping on Ag/Sbad/Sead underlayer and on individual antimony and selenium below. After anodic stripping returns the electrode to its low-capacitive state, Snad deposition raises the Qdl. Snad denudation from chalcogen adsorbed layers is headed by an extra enhance in Qdl, similar to Snad stripping from bulk Antimony as notified in [33], although this result is not typical of Snad stripping from a composite bilayer. Since the reduced status of Qdl is more closely maintained by the Ag/Sbad/Sead underlayer, the amplitude of Qdl fluctuation in Sn upd cycles is about three times smaller than the Qdl variation in Sn underpotential deposition on separate Antimony and selenium adlayers. A strong hysteresis in the Qdl difference of the potential cycle clearly demonstrates the irreversible nature of Sn underpotential deposition on Ag/Sbad/Sead.

In Sn underpotential deposition on a bilayer and individual chalcogen adlayers, the characteristics of the Faradaic component of impedance are likewise highly self-descriptive (Fig. 4a and b). While Aw(E) is most noticeable during the stripping stage, Rct(E) is particularly vulnerable to Sn deposition on Ag/Sbad/Sead. Fig. 4 b is lacking the matching curve because charge transfer resistance contributes very little to impedance in Sn underpotential deposition on selenium adlayer. Sn underpotential deposition on a bi-chalcogen underlayer has an order of magnitude more inverse charge transfer resistance than Sn upd on a single antimony adlayer. Using selenium in the adlayer allows for faster Sn upd kinetics, which can be taken advantage of in monitoring multilayer assemblies. Figure 4c shows that the main peak in A−w1(E) is highly indicative of

selenium in the underlayer and this aspect of the ac response is particularly valuable when conducting an anodic scan.

4. TYPICAL PARAMETER VARIATIONS WITH ELECTRODE POTENTIAL

4.1 $Ag/Sb_{ad}/Se_{ad}/Sn_{ad}$

Voltammograms of Ag underpotential deposition on Ag/Se_{ad}, Ag/Sb_{ad}, and $Ag/Sb_{ad}/Se_{ad}$ are displayed in Fig. 5. Ag upd displays a high degree of irreversibility on all of these substrates. Around 65 mV higher than the Nernst potential of bulk Ag deposition, the electrical potential of Ag on Ag/Se_{ad} begins at around 160 mV. The cathodic peak is at 110 mV and the anodic peak is at 280 mV, as shown in Figure 5a. Figure 5b and c indicate that the anodic scan on Ag/Sb_{ad} reveals a peak, but the cathodic scan reveals just a shoulder at varying scanning rates. With a decrease in the scan rate from 52 to 6mV/s, the anodic charge rises from 198 to 362μCcm^2 in a sequence of voltammograms displayed in Fig. 5c. Figure 5c also shows a CV for Ag on Ag, which shows that the anodic peak of $Ag/Sb_{ad}/Ag_{ad}$ is more positively positioned than bulk Silver. It is possible that the lower potential of the Ag anodic peak on Ag/Sb_{ad} and the less noticeable Ag upd on Ag/Sead are due to the fact that the synthesis of tellurides requires less negative free energy than selenides, which had a comparable effect on the Zn underpotential deposition potential on Gold covered with various chalcogen adlayers [34].

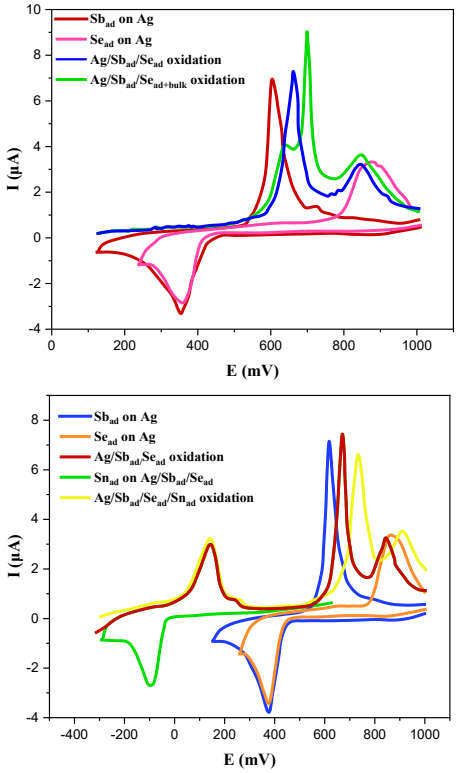

Figure 3. Voltammograms delineating phases of atomic three-layer assembly of $Ag/Sb_{ad}/Se_{ad}/Sn_{ad}$. Acquired Analytical stripping voltammograms using the identical solutions utilized in the adlayer deposition process. dE/dt = 78 mV/s.

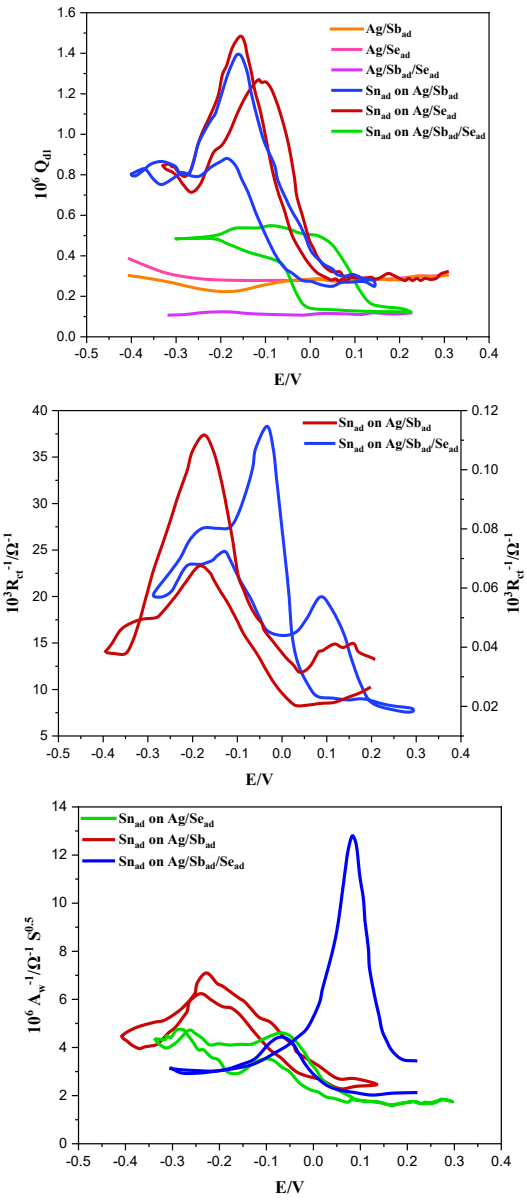

Figure 4. Equivalent circuit parameters for Sn update on Ag/Sbad/Sead bilayer in 0.1M HClO4: pseudo-capacitance of double electric layer, inverse resistance of charge transfer, and coefficient of Warburg across curvature 1 (Ag/Sbad), 2 (Ag/Sead), and 3 (Ag/Sbad/Sead) at a scan rate of 2.7mV/s.

4.2 $Ag/Sb_{ad}/Se_{ad}/Ag_{ad}$

The cathodic scan of composite bilayer revealed a shoulder prior to switch to bulk deposition of Ag. Anodic oxidation showed no preference for silver deposited under upd or overpotential deposition (opd) conditions. This is because the chalcogen support allows the silver atoms to penetrate, a phenomenon that is typical of Ag deposition on bulk Sb [35-38]. Because of the interaction between Ag and chalcogen, the voltammograms of Sb and Se anodic stripping look very different from the corresponding voltammograms in Sn underpotential deposition, and these differences are depending on the conditions of silver deposition. On Ag/Sead and Ag/Sbad/Sead, Qdl(E) demonstrates cyclic scans with

recognizable hysteresis loops, while on Ag/Sbad, a more intricate variation in upd is observed. In the second scenario, the impacts of rapid interaction between the underlayer and Ag adatoms are shown by a burst of capacitive response in the upd range.

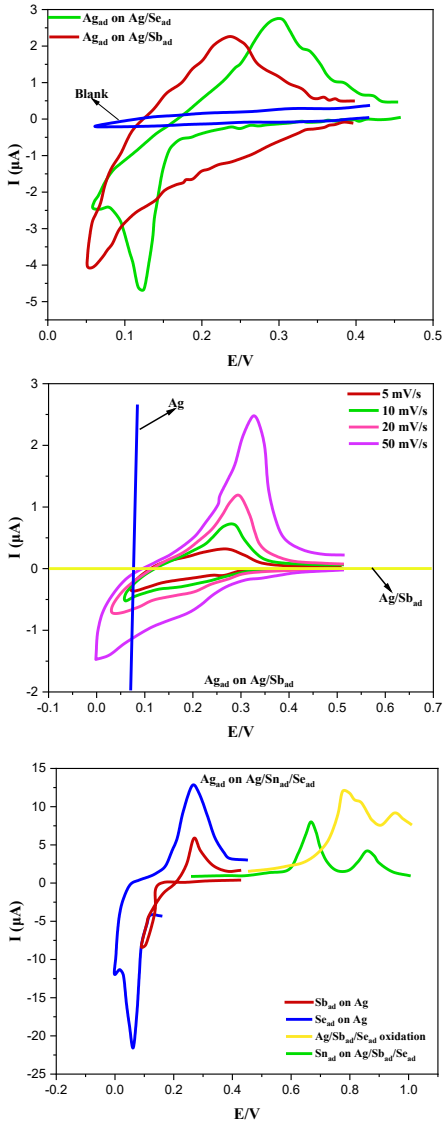

Figure 5. Cyclic voltammograms showcasing Ag underpotential deposition on various layers: (a) Ag_{ad} on Ag/Sbad/Sead, (b) Ag_{ad} on Ag/Sbad and (c) Ag_{ad} on $Ag/Sn_{ad}/Sn_{ad}$. Curves 1 and 2 in (c) depict Ag formation and stripping, curve 3 shows stripping of a composite deposit formed over three cycles, and curve 4 details the removal of Ag/Sbad/Sead post-assembly. Scan rates are 78mV/s except in (c), shown in the image. Electrolyte used is 0.1M HClO4 with 10mM Ag(ClO4)2

To make up for the unimpressive CV—which does not display an underpotential deposition peak in the cathodic scan—the dependences of equivalent electric circuits variables on electrode potential shows upd peaks. A greater contribution to the admission of the Faradaic component of the ac response is likewise produced by Ag interaction with Sb (Fig. 6). In contrast, the existence of selenium dictates the Faradaic component of admission within the spectrum of silver oxidation. In electroactive multilayers, this case study shows that multiparametric ac response is better than one-dimensional dc response. It is possible to have a better grasp of and control over the nonstationary processes present in interfaces that seem uninteresting in cyclic voltammetry by using multiparametric ac monitoring to reveal numerous hidden dependencies.

Chalcogen atomic layers and bilayers containing silver adatoms are an ancient type of electroactive material with complex electrochemical, chemical charging, and diffusional processes. This system is not very good at producing stable structures with more than a few atomic layers due to the mobility of silver in the chalcogen composite layer. Conversely, regulating the electrochemical production of interfacial nanostructures may still involve the rapid interaction of adatoms with chalcogen.

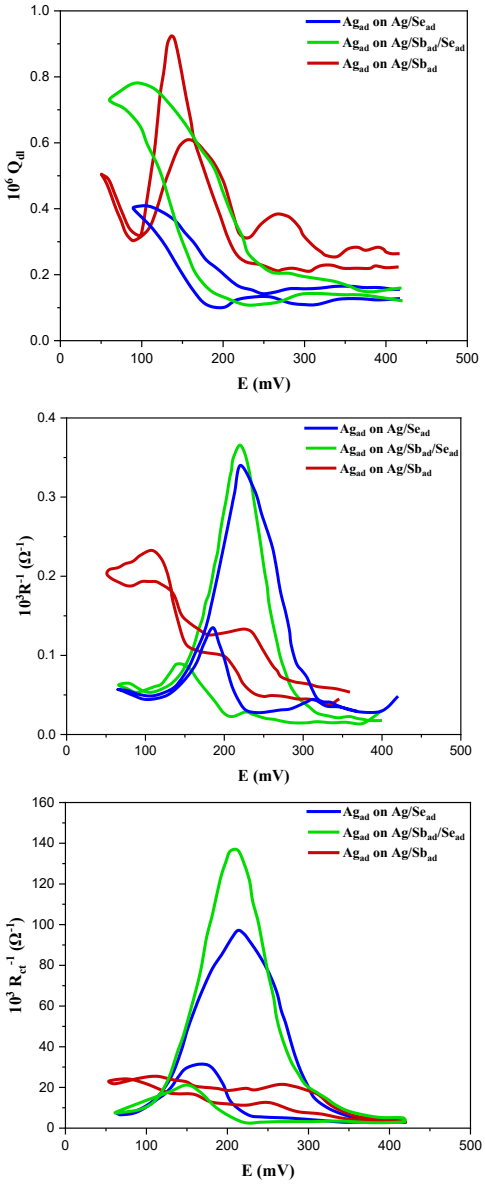

Figure 6. Optical potential distribution (opd) and equivalent circuit variables change in Ag underpotential deposition on Se, Sb, and Sb-Se atomic bilayers.

4.3 Ag/Sb$_{ad}$/Zn$_{ad}$

Zinc plating on antimony atomic layers is one step in the sequential fabrication of ZnSb nanomaterials. The fluctuation of Qdl during the deposition of Antimony adlayer on Silver and the subsequent deposition of Znad onto Ag/Sbad is illustrated in Fig. 7a. While depositing an antimony adlayer, the capacitance of the silver electrode drops by a factor of one, from its initial high value. While the shift in Qdl during Zn upd, the following step of multilayer assembly, is not as substantial as it is during Sbad deposition, it is still enough to monitor the interface's dynamic condition. In addition to being able to track events occurring at the interface, the data on kinetic variables, such as the charge transfer resistance and Warburg coefficient, may be acquired concurrently with Qdl (Fig. 7b). Changes in the Warburg coefficient and the charge transfer resistance were both useful for monitoring the interface in this system, and they were also highly connected with one another.

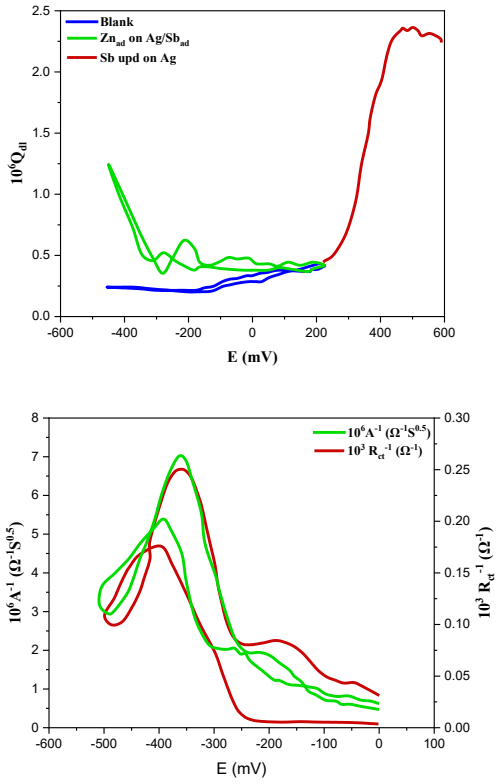

Figure. 7. (a) Q_{dl}, (b) R_{-ct}^{1}, and A_{-w}^{1} difference in potential of cyclic scan in Zn underpotential deposition on Ag/Sb$_{ad}$.

5. CONCLUSIONS

The phrase "potentiodynamic electrochemical impedance spectroscopy" describes an experiment that uses a set of parameters normally used in stationary impedance spectroscopy but is controlled by potentiodynamic. All of the parameters in Potentiodynamic electrochemical impedance spectroscopy spectra analysis, similar to straight current in CV are functions of the electrode potential. The Potentiodynamic electrochemical impedance spectroscopy spectra provide these additional potentiodynamic curves, which describe the ac response in their own unique way. Electroactive particle diffusion, interfacial charge transfer, and the presence of a double layer are the three variables typically provided by PDEIS in the irreversible upd. The article's several examples show that the electrochemical atomic layer-by-layer deposition method can extract all parameters at once by analyzing impedance data from the same device (potentiostat) used to control the potential scan. In order to learn about different parts of the interface dynamics, it is not necessary to significantly disrupt the system. Although there are currently no major limitations to conducting PDEIS spectrum analysis in real-time, the current version of PDEIS does so after the scan. With the potential scan's multiparametric monitoring of interface activities, we anticipate that electrochemical multilayer assembly control will be much easier.

REFERENCES

[1] Marcin Basiaga, Witold Walke, Anna Taratuta, Julia Lisoń, Agata Sambok-Kiełbowicz, Wojciech Kajzer, Magdalena Szindler, Klaudiusz Gołombek & Alina Domanowska, 2022 “Electrochemical Behavior of SnO2 Layer Deposited on Biomaterials Used in Bone Surgery,” in *Advanced Structured Materials*, vol. 172, pp. 39–58. DOI: 10.1007/978-3-030-97925-6_4

[2] M. Fedel, C. Zanella, S. Rossi, and F. Deflorian, 2014, “Corrosion protection of silver coated reflectors by atomic layer deposited Al2O3,” *Solar Energy*, vol. 101, pp. 167–175. DOI: 10.1016/j.solener.2013.11.038

[3] I. Spajić, E. Rahimi, M. Lekka, R. Offoiach, L. Fedrizzi, and I. Milošev, 2021 “Al2O3and HfO2Atomic Layers Deposited in Single and Multilayer Configurations on Titanium and on Stainless Steel for Biomedical Applications,” *J Electrochem Soc*, vol. 168, no. 7. DOI: 10.1149/1945-7111/ac131b

[4] M. Staszuk, 2023, “Investigations of CrN/TiO2 coatings obtained in a hybrid PVD/ALD method on Al–Si–Cu alloy substrate,” *Bulletin of the Polish Academy of Sciences: Technical Sciences*, vol. 71, no. 2. DOI: 10.24425/bpasts.2023.144622

[5] I. Spajić, P. Rodič, G. Šekularac, M. Lekka, L. Fedrizzi, and I. Milošev, 2021, “The effect of surface preparation on the protective properties of Al2O3 and HfO2 thin films deposited on cp-titanium by atomic layer deposition,” *Electrochim Acta*, vol. 366. DOI:10.1016/j.electacta.2020.137431

[6] S. Venkatesa Prabhu, G. Ramesh, A. T. Adugna, S. M. Beyan, and K. Gizachew Assefa, 2019, “Kinetics of iron bioleaching using isolated leptospirillum ferriphilum: Effect of temperature,” *International Journal of Innovative Technology and Exploring Engineering*, vol. 8, no. 12, pp. 76–81. DOI: 10.35940/ijitee.L3210.1081219

[7] Fatma Mohamed Mahgoub1,2*, S. M. Al-Rashdi3, 2016 “Investigate the Corrosion Inhibition of Mild Steel in Sulfuric Acid Solution by Thiosemicarbazide,” Journal of Physical Chemistry, vol. 6, pp. 54-66. DOI:10.4236/ojpc.2016.63006

[8] Wenshu Li, Bingfeng Wang, Xiaoxia Huang, Bin Liu, Jamieson Brechtl, Peter K. Liaw, Mechanical behavior and shear band of a powder-metallurgy-fabricated CoCrFeMnNi high-entropy alloy during high strain-rate deformation, Journal of Materials Research and Technology, Volume 21, 2022, Pages 1461-1478, DOI:10.1016/j.jmrt.2022.09.106.

[9] Vijayakumar Arun, R. Kannan, S. Ramesh, M. Vijayakumar, P. S. Raghavendran, M. Siva Ramkumar, P. Anbarasu, Venkatesa Prabhu Sundramurthy, 2022 "Review on Li-Ion Battery vs Nickel Metal Hydride Battery in EV," *Advances in Materials Science and Engineering*, vol. 2022. DOI: 10.1155/2022/7910072

[10] Naser Ali 1,2,* , Joao A. Teixeira 1 , Abdulmajid Addali 1 , Maryam Saeed 2 , Feras Al-Zubi 2 , Ahmad Sedaghat 3,4 and Husain Bahzad 5, 2019, "Deposition of Stainless Steel Thin Films, Vol 12, No 4. PP-571, DOI:10.3390/ma12040571

[11] I. S. N. V. R. Prasanth, Prabahar Jeevanandam, P. Selvaraju, K. Sathish, S. K. Hasane Ahammad, P. Sujatha, M. Kaarthik, S. Mayakannan, Bashyam Sasikumar, 2023, "Study of Friction and Wear Behavior of Graphene-Reinforced AA7075 Nanocomposites by Machine Learning", Journal of Nanomaterials, vol. 2023, Article ID 5723730, 15 pages. DOI:10.1155/2023/5723730

[12] S. Mayakannan, R. Rathinam, Rajasekaran Saminathan, R. Deepalakshmi, Mahesh Gopal, J. Justin Maria Hillary, S. Nanthakumar, V. Y. Ganvir, Pallavi Singh, 2022, "Analysis of Spectroscopic, Morphological Characterization and Interaction of Dye Molecules for the Surface Modification of TiB2 Nanoparticles", Journal of Nanomaterials, vol. 2022, Article ID 1033216, 9 pages. DOI: 10.1155/2022/1033216

[13] T. A. Amibo, S. M. Beyan, M. Mustefa, V. P. Sundramurthy, and A. B. Bayu, 2022, "Development of Nanocomposite based Antimicrobial Cotton Fabrics Impregnated by Nano SiO2 Loaded AgNPs Derived from Eragrostis Teff straw," *Materials Research Innovations*, vol. 26, no. 7, pp. 405–414. DOI: 10.1080/14328917.2021.2022372

[14] Venkatramanan Varadharajan, Dilip Saravanan Senthilkumar, Kathiresan Senthilkumar, Venkatesa Prabhu Sundramurthy, Rahul Manikandan, Hariprasath Senthilarasan, Harish Ganesan, Indiravadanan Kesavamoorthy, Arulvel Ramasamy, 2022, "Process modeling and toxicological evaluation of adsorption of tetracycline onto the magnetized cotton dust biochar," *Journal of Water Process Engineering*, vol. 49. DOI:10.1016/j.jwpe.2022.103046

[15] M. Staszuk, D. Pakuła, Ł. Reimann, A. Kloc-Ptaszna, M. Pawlyta, and A. Kříž, 2021, "Structure and properties of TiO2/nanoTiO2 bimodal coatings obtained by a hybrid PVD/ALD method on 316L steel substrate," *Materials*, vol. 14, no. 16. DOI: 10.3390/ma14164369

[16] E. T. Akinlabi, A. D. Baruwa, O. P. Oladijo, N. Maledi, and J. Chinn, 2019, "Characterization of Hydrophobic Silane Film Deposited on AISI 304 Stainless Steel for Corrosion Protection," *J Mater Eng Perform*, vol. 28, no. 10, pp. 6330–6339. DOI: 10.1007/s11665-019-04349-9

[17] Sankar, L.P., Kamalakannan, R., Aruna, G., Meera, M.R., Vijayan, V., Sivananthan, S. (2020). Mechanical behavior and microstructure evolution of Al-5%Cu/TiC metal matrix composite. Journal of New Materials for Electrochemical Systems, Vol. 23, No. 4, pp. 252-255. DOI: 10.14447/jnmes.v23i4.a05

[18] B. Ramesh, S. Sathish Kumar, A. H. Elsheikh, S. Mayakannan, K. Sivakumar, and S. Duraithilagar, "Optimization and experimental analysis of drilling process parameters in radial drilling machine for glass fiber/nano granite particle reinforced epoxy composites," in *Materials Today: Proceedings*, Elsevier Ltd, 2022, pp. 835–840. DOI: 10.1016/j.matpr.2022.04.042

[19] Roseline, S., Paramasivam, V., Parameswaran, P., Antony, A.G. (2019). Evaluation of mechanical properties and stability of Al 6061 with addition of ZrO2 And Al2O3. Journal of New Materials for Electrochemical Systems, Vol. 22, No. 1, pp. 21-23. DOI: 10.14447/jnmes.v22i1.a05

[20] P. Muruganandhan, S. Jothilakshmi, R. Vivek, S. Nanthakumar, S. Sakthi, S. Mayakannan, R. Girimurugan, 2023, "Investigation on silane modification and interfacial UV aging of flax fibre reinforced with polystyrene composite," *Mater Today* DOI; 10.1016/j.matpr.2023.03.272

[21] Mirco Peron, Susanna Cogo, Maria Bjelland, Abdulla Bin Afif, Anup Dadlani, Elisa Greggio, Filippo Berto, Jan Torgersen, 2021, "On the evaluation of ALD TiO2, ZrO2 and HfO2 coatings on corrosion and cytotoxicity performances," *Journal of Magnesium and Alloys*, vol. 9, no. 5, pp. 1806–1819. DOI: 10.1016/j.jma.2021.03.010

[22] A. Ziębowicz, A. Woźniak, B. Ziębowicz, K. Kosiel, and G. Chladek, "The effect of atomic layer deposition of ZrO2 on the physicochemical properties of cobalt based alloys intended for prosthetic dentistry," *Archives of Metallurgy and Materials*, vol. 63, no. 3, pp. 1077–1082, 2018. DOI: 10.24425/123778

[23] Mohanasundaram Sugumar , Varadharajan Venkatramanan, Selvaraju Mayakannan, Manikandan S, Subbaiya Ramasamy, Jayakumar Mani, Sundaramurthy Venkatesa Prabhu, Gurunathan Baskar , Pugazhendhi Arivalagan, 2024, "Green ammonia as peerless entity for realm of clean-energy carrier toward zero carbon emission: Purviews, neoteric tendencies, potentialities and downsides," *Fuel*, vol. 365. DOI: 10.1016/j.fuel.2024.131118

[24] X. Guo, K. Du, Q. Guo, Y. Wang, R. Wang, and F. Wang, 2013, "Study of barrier property of composite film coated on mg-gd-y alloy bywater Diffusion," *ECS Electrochemistry Letters*, vol. 2, no. 8, pp. C27–C30. DOI: 10.1149/2.004308eel

[25] W. Kajzer, A. Kajzer, M. Grygiel-Pradelok, A. Ziębowicz, and B. Ziębowicz, 2016, "Evaluation of physicochemical properties of TiO2 layer on AISI

316LVM steel intended for urology," in *Advances in Intelligent Systems and Computing*, pp. 385–398. DOI: 10.1007/978-3-319-39904-1_34

[26] Y. Zhu, Y. Xu, S. Song, X. Wang, G. Liu, and Y. Huang, 2020, "Probing the nonuniform corrosion of pipeline weldments under stepwise increasing solution temperature using a coupled multielement electrical resistance sensor," *Materials and Corrosion*, vol. 71, no. 8, pp. 1386–1399. DOI: 10.1002/maco.201911462

[27] Loganathan, M., Dinesh, S., Vijayan, V., Karuppusamy, T., Rajkumar, S. (2020). Investigation of mechanical behaviour on composites of Al6063 alloy with silicon, graphite and fly ash. Journal of New Materials for Electrochemical Systems, Vol. 23, No. 1, pp. 36-39. DOI: 10.14447/jnmes.v23i1.a07

[28] Ahmed J. Hassan 2014, "Study of Optical and Electrical Properties of Nickel Oxide (NiO) Thin Films Deposited by Using a Spray Pyrolysis Technique," Journal of Modern Physics, 2014, vol. 5, pp. 2184-2191. DOI:10.4236/jmp.2014.518212

[29] B. M. Cerrutti, M. L. Moraes, S. H. Pulcinelli, and C. V Santilli, 2015, "Lignin as immobilization matrix for HIV p17 peptide used in immunosensing," *Biosens Bioelectron*, vol. 71, pp. 420–426. DOI: 10.1016/j.bios.2015.04.054

[30] R. Rudolf, A. Stambolić, and A. Kocijan, 2021, "Atomic layer deposition of atio2 layer on nitinol and its corrosion resistance in a simulated body fluid," *Metals (Basel)*, vol. 11, no. 4. DOI: 10.3390/met11040659

[31] Z. Xu, Q. Zhang, L. Luo, Y. Liu, and J. Wan, 2021, "Microstructure and corrosion resistance of TiN/TiO2 nano-composite film on AZ31 magnesium alloy," *Surf Coat Technol*, vol. 406. DOI: 10.1016/j.surfcoat.2020.126681.

[35] M. Fedel and F. Deflorian, 2016, "Electrochemical characterization of atomic layer deposited Al2O3 coatings on AISI 316L stainless steel," *Electrochim Acta*, vol. 203, pp. 404–415. DOI 10.1016/j.electacta.2016.02.107

[36] S.Dinesh, A.Godwin Antony, S.Karuppusamy, V.Vijayan and B.Suresh Kumar, 2016. Experimental investigation and optimization of machining parameters in CNC turning operation of duplex stainless steel. Asian Journal of Research in Social Sciences and Humanities 6,pp. 179-195. DOI: 10.5958/2249-7315.2016.01006.6

[37] S.Dinesh, A.Godwin Antony, K.Rajaguru and V.Vijayan. 2016. Investigation and Prediction of material removal rate and surface roughness in CNC turning of EN24 alloy steel, Asian Journal of Research in Social Sciences and Humanities , vol 6 (8) 849—863. DOI:10.5958/2249-7315.2016.00654.7

[38] T.Tamizharasan, N.Senthil Kumar, V.Selvkumar, S.Dinesh, 2019. Taguchi's Methodology of optimizing turning parameters over chip thickness ratio in machining PM AMMC, SN Appl. Sci. 1: 160., Springer Publishers.DOI 10.1007/s42452-019-0170-8